ADVANCED FUNCTIONAL MATERIALS
www.afm-journal.de

Following Chemical Charge Trapping in Pentacene Thin Films by Selective Impurity Doping and Wavelength-Resolved Electric Force Microscopy

*Louisa M. Smieska, Vladimir A. Pozdin, Justin L. Luria, Richard G. Hennig, Melissa A. Hines, Chad A. Lewis, and John A. Marohn**

Charge trapping is one of several factors that limit the performance of organic electronic materials, yet even in pentacene, a prototypical small-molecule semiconductor, the precise chemical nature of charge trapping remains poorly understood. Here the effects of three chemical trap-precursor candidates are examined by layering thin-film pentacene transistors with different pentacene defect species. The resulting charge trapping is studied in each device via scanning-probe electric force microscopy coupled with variable-wavelength sample illumination. Firstly, it is found that layering with pentacen-6(13H)-one (PHO) readily produces uniform charge trapping everywhere in the transistor channel, as expected for an active blanket-deposited trap-precursor. However, layering with 6,13-dihydropentacene (DHP) produces fewer, more-isolated traps, closely resembling the surface potential distribution in pristine pentacene thin films. Secondly, the rates of trap-clearing versus illuminating wavelength (trap-clearing spectra) are measured, revealing enhanced trap-clearing rates at wavelengths assigned to the absorption of either pentacene or the charged trap species. The trap-clearing spectrum for the PHO-layered sample closely resembles the spectrum obtained from pentacene aged in a working transistor, while the trap-clearing spectrum for the DHP-layered sample resembles the spectrum observed in pristine pentacene. We conclude that PHO competently creates traps in pentacene that match the expected trap-clearing spectrum for degraded pentacene, while DHP does not, and that the chemical trap species in aged pentacene is very likely PHO^+.

1. Introduction

Degradation is an acknowledged issue in organic semiconductors that decreases the amount of active material and creates impurities. However, the distinction between degradation alone and degradation that affects performance is often lacking. In many cases, impurities in organic semiconductors are proposed as a source of charge trapping. Intentional doping with impurities for controlled charge trapping is important for optimizing applications like photorefractive materials[1,2] and organic transistor memory.[3] Conversely, in organic transistors and most other applications of organic semiconducting materials, charge trapping is detrimental to device performance because it increases operating voltages and decreases mobility.

There are hundreds of characterized organic semiconducting materials, but only a few systems in which the chemical degradation product responsible for decreased performance has been spectroscopically identified.[4,5] Even the most sensitive bulk materials characterization techniques can only demonstrate the presence of impurities and may not be capable of detecting defects at concentrations relevant to device performance.[6] Few characterization techniques can draw a direct connection between the presence of impurities and regions of decreased performance. For example, although XPS is an extremely sensitive surface analysis technique, it does not necessarily yield information about the semiconductor-dielectric interface, where most of charge transport occurs. There is a need for techniques that can provide local information correlating threshold voltage and chemical composition. The work presented in this paper is designed to deepen our understanding of chemical charge trapping in pentacene. First, we directly deposit possible chemical trap-precursor molecules on top of very thin pentacene films in a bottom-contact transistor geometry (**Figure 1**a). We then measure the resulting spatial distribution of charge trapping in the transistor channel (Figure 1b). Finally, we spectroscopically probe the electronic energy levels in the cationic trap species by introducing variable-wavelength sample illumination (Figure 1c). These experiments allow us to directly microscopically and spectroscopically investigate the charge-trapping efficacy of various chemical defects in pentacene. We find that the charged species responsible for charge trapping in aged pentacene is very likely PHO^+.

L. M. Smieska, J. L. Luria, M. A. Hines, C. A. Lewis, J. A. Marohn
Department of Chemistry and Chemical Biology
Cornell University, Ithaca
NY 14853, USA
E-mail: jam99@cornell.edu
V. A. Pozdin, R. G. Hennig
Department of Materials Science and Engineering
Cornell University
Ithaca, NY 14853, USA

DOI: 10.1002/adfm.201200595

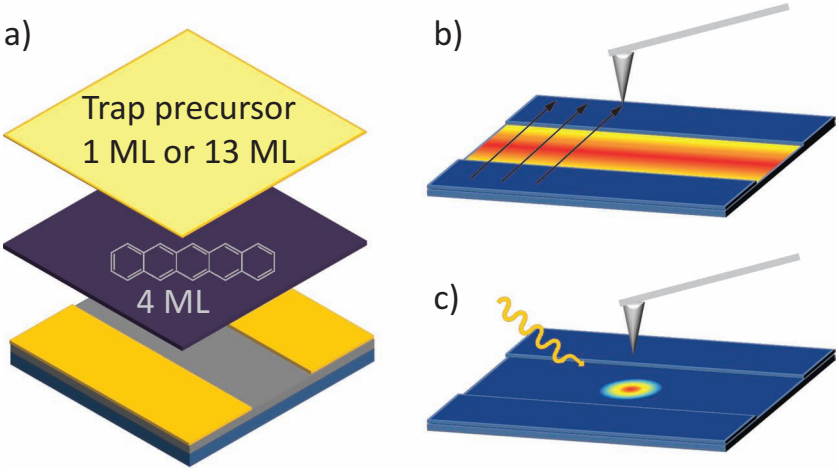

Figure 1. a) Schematic of samples investigated in this study: 4 monolayers (4 ML) of pentacene were deposited on bottom-contact transistor substrates and subsequently layered with 1 ML or 13 ML of a trap-precursor defect species. b) Schematic of electric force microscopy (EFM) surface potential mapping. The local threshold voltage is measured as the contact potential difference between the cantilever tip and the sample surface while the cantilever is scanned in-plane above the sample. c) Schematic of time- and wavelength-resolved EFM trap-clearing experiments. The cantilever is positioned above a single point of interest and the local contact potential difference is measured as a function of time while the sample is illuminated from above with monochromatic light. The cantilever is not scanned in the lateral plane during this measurement. The cantilever does not contact the sample in either (b) or (c).

To perform the charge trapping characterization described above (Figure 1b,c), we employ electric force microscopy (EFM). EFM is a non-perturbative scanning-probe technique that measures the contact potential difference between a metallic cantilever tip and the sample below.[7] EFM has been used to image charged traps in thin films of pentacene and pentacene derivatives.[8,9] Recently, Luria et al. have demonstrated that EFM can also be used to spectroscopically measure the energy levels of the charged trap species in aged pentacene.[10] Charged traps in pentacene are neutralized by electron transfer from neighboring molecules. This process is very slow (many hours) when driven by thermal energy, but it can occur at a faster rate (seconds) under illumination.[11] This rate enhancement is usually attributed to photoexcitation of pentacene followed by electron transfer to the trap. Luria et al. measured the local surface potential of a charged trap in aged pentacene as a function of time while illuminating the sample from above. By extracting the trap-clearing rate as a function of illuminating wavelength, Luria et al. revealed that the rate of trap-clearing in pentacene is enhanced at 500 nm. 500 nm does not correspond to a strong pentacene absorption, indicating the existence of a second trap-clearing mechanism. The peak at 500 nm in the spectrum of light-induced trap-clearing rate was smooth and symmetrical, which suggested that it might arise from excitation of a single chemical species, consistent with other observations that hole traps in pentacene arise from a discrete oxygen-related defect.[12,13] To explain these observations, a new internal photoexcitation mechanism of trap-clearing was proposed, involving direct absorption by the charged trap species (rather than pentacene) followed by electron transfer from pentacene and neutralization of the trap.[10] The trap-clearing spectrum thus measures an electronic transition in the cationic trap species. In the present work, we add chemical defect species to pristine pentacene transistors and compare their trap-clearing spectra to the spectrum obtained from aged pentacene.

In the following two paragraphs, we evaluate a few of the numerous possibilities for the proposed chemical charged trap species. Exposure of pentacene films to humidity leads to charge trapping[14] and produces a variety of oxygenated species observable by mass spectrometry.[15] In solution, the reaction of pentacene with oxygen to form an endoperoxide has been known for decades,[16] and many computational studies affirm this reactivity.[17,18] However, the pentacene endoperoxide is highly distorted out of plane,[19] and calculations indicate that it is not the most stable oxygen-related defect in the pentacene crystal.[20] Although the analogous endoperoxide has been proposed in rubrene single crystals as a product of exposure to light and oxygen,[21] this species is unstable in the crystal by at least 1.1 eV compared to other oxygen related defects.[22,23] It has been shown that pentacene stability and photochemistry is very different in solution versus in thin films,[17] and XPS studies of pentacene photooxidation in thin films suggested that the endoperoxide in pentacene films is probably converted to a more stable species.[24] To our knowledge, the pentacene endoperoxide has not been spectroscopically observed as a degradation product in polycrystalline pentacene thin films. For these reasons, the endoperoxide was not considered as a trap precursor in this study, but we do consider two other oxygenated species as trap precursors, discussed below (pentacen-6(13H)-one, PHO; 6,13-pentacenequinone, PQ; **Figure 2**a).

Hydrogenated pentacene defects have been predicted computationally[25] and observed experimentally as byproducts of pentacene sublimation via mass spectrometry,[26,27] and possible mechanisms for the process of hydrogenation have also been studied computationally.[28] Northrup and Chabinyc noted that pentacene is energetically likely to have a dihydrogen defect ($C_{22}H_{16}$, or DHP, Figure 2a), and they also suggested several oxygenated traps and neutral defects ($C_{22}H_{13}O$, $C_{22}H_{15}O$ and $C_{22}H_{16}O$, not pictured), predicting that defects like these will give rise to gap states and could form charged defects in the presence of pentacene cation radicals.[25] Considerable attention has also been paid to the impurity 6,13-pentacenequinone ($C_{22}H_{12}O_2$, PQ, Figure 2a) identified in commercial pentacene.[29] The presence of PQ in pentacene films has been shown to have a significant effect on mobility,[29,30] island nucleation,[31] and thin film morphology.[30,32,33] However, the precise role of PQ in these effects remains unclear. PQ's energy levels suggest that it behaves as a scattering center rather than a charged trap species,[29] but its geometry and distribution in the film are consistent with the possibility of charged traps due to structural defects.[30] Finally, the so-called "butterfly" photodimer of pentacene has been characterized by UV/Vis spectroscopy in solution and in PMMA films.[34] Analogous dimers of trialkylsilylalkynyl-functionalized

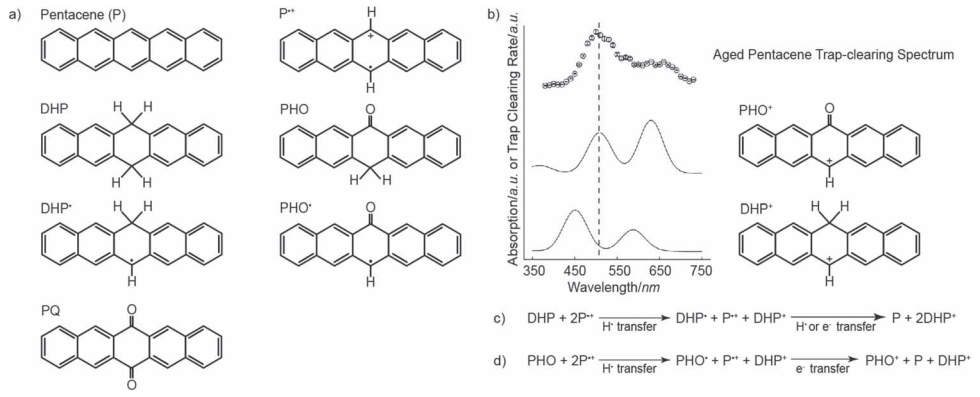

Figure 2. a) Molecules, intermediates, and charged species. $P^{\bullet+}$ is a pentacene hole carrier. DHP and PHO are neutral trap-precursor candidates that may undergo hydrogen-atom loss followed by electron loss. PQ is a major impurity in commercial pentacene. b) Trap-clearing spectrum obtained from aged pentacene compared with calculated absorption spectra for the proposed charged trap species, PHO^+ and DHP^+. Reproduced with permission.[10] c) Proposed mechanism for the formation of DHP^+ from DHP. d) Proposed mechanism for the formation of PHO^+ from PHO. Note that DHP^+ is formed in both mechanisms (c) and (d). The calculated thermodynamics and proposed mechanisms for processes (c) and (d) have been previously reported in the Supporting Information of Luria et al.[10]

pentacene have been characterized in solution and thin films,[35] and silylethyne-substituted hexacenes are known to undergo dimerization in solution and in the solid state.[36] To the best of our knowledge, the pentacene dimer has not been spectroscopically observed in thin films. For this reason, and because we did not observe any species of such high molecular weight by mass spectrometry of our samples, we did not consider the pentacene butterfly dimer as a possible trap precursor.

Luria et al. assessed several charged trap species by considering the electronic transition measured in the trap-clearing spectrum of aged pentacene. Challenging time-dependent density functional theory calculations of the charged species' absorption spectra were performed by Schwarz and Hennig.[10] By comparing the experimental pentacene trap-clearing spectrum with the calculated absorption spectra (Figure 2b), Luria et al. found that pentacen-6(13H)-one (PHO) and 6,13-dihydropentacene (DHP) were likely candidates for chemical trap-precursors in pentacene. Proposed mechanisms for the formation of the charged trap species from the neutral precursors are summarized in Figure 2c,d.[25,10] Note that the degradation of DHP (Figure 2c) results only in DHP^+, while the degradation of PHO (Figure 2d) is expected to produce both DHP^+ and PHO^+.

The literature suggests two possible methods for intentionally adding impurities to sublimed pentacene thin films. Impurity molecules can be co-deposited with pentacene by physically mixing them as solids and then depositing the mixture itself.[30] Alternatively, impurity molecules can be sequentially deposited on top of very thin layers of pentacene (4 monolayers, 4 ML).[32] We chose to sequentially deposit the impurities on the pentacene since this allowed us to separately analyze the success of each deposition as well as to monitor the condition of the added precursor compound before and after being heated for deposition. In our case, both deposition methods are intended to incorporate the additive precursor into the first few critical monolayers where charge is transported so it can react with pentacene cation radicals (charge carriers) to form a charged trap species. The critical thickness at which mobility saturates is thought to represent the number of monolayers that contribute to charge transport; this thickness is also known as the Debye length. In pentacene, measurements of this thickness range from 2 ML to 6 ML.[37–41] For deposition conditions nearly identical to ours, Shehu et al. measured a critical thickness of 4 ML, suggesting that our 4 ML films should be saturated with pentacene cation radicals when a negative gate bias is applied.[42] In this case, we would expect the reaction of the neutral trap precursor with pentacene hole carriers to take place uniformly throughout the transistor channel; this hypothesis is supported by the uniform trapping by PHO in **Figure 3**d. Our samples are thus designed such that trap precursors are not required to intercalate into the pentacene layer to react with the hole carriers, i.e., pentacene cation radicals are expected to be available at the interface between the pentacene and the trap precursor.

In the present work, we layer pristine pentacene transistors with three different possible trap-precursors. We study PHO and DHP based on the predictions of Luria et al. and also PQ (despite its unfavorable trapping energetics) since it is the starting material for the synthesis of PHO. We note that although the tautomer of PHO considered as a trap-precursor by Northrup and Chabinyc may be more likely to form in aged pentacene films than PHO since it does not break resonance, both precursors are expected to yield PHO^+ in the presence of pentacene cation radicals.[25,10] The goal of this work is to compare the trap-clearing spectra in these intentionally "doped" samples with the theoretical predictions of Luria et al. and with the trap-clearing spectrum in undoped aged pentacene to reveal the chemical identity of the charged trap species. Below, we use EFM to measure spatial distribution of charge trapping and trap-clearing spectra of pentacene transistors with the three trap-precursors of interest. We use mass spectrometry and IR spectroscopy to corroborate the presence of the impurities in the transistor channel. Our data strongly supports PHO^+ as the charged trap species in aged pentacene.

2. Results

Figure 3 shows the results of our AFM and modulated EFM imaging measurements. In the AFM images, Figure 3g–i,

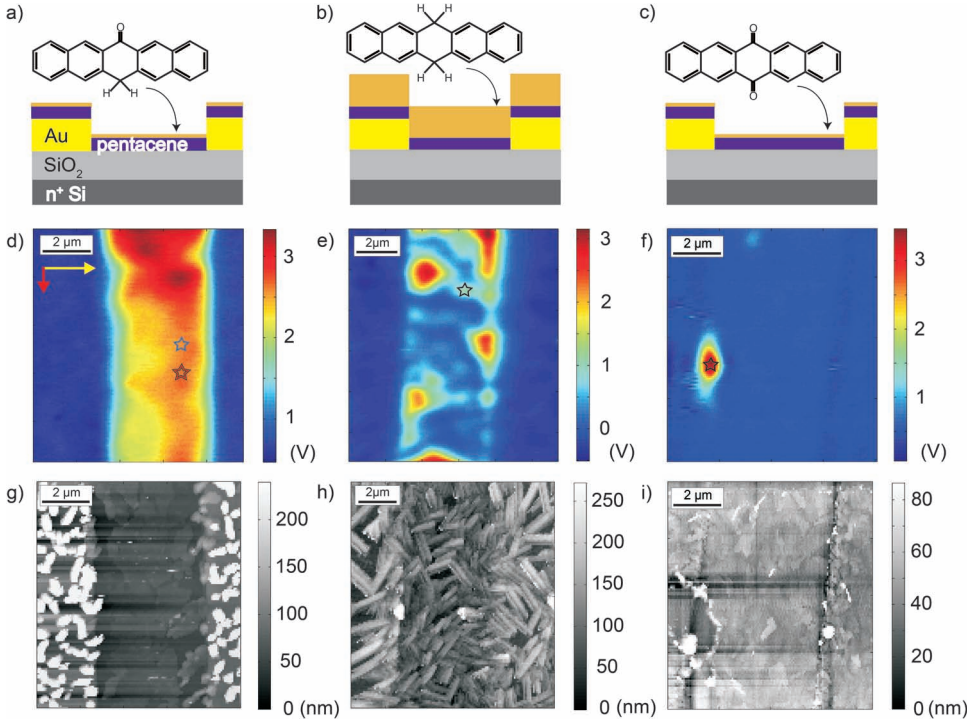

Figure 3. a–c) Schematic side views of the sequentially deposited bottom-contact transistor substrates used in this work. The trap-precursor molecules shown are: a) 1 ML PHO; b) 13 ML DHP, and c) 1 ML PQ deposited on top of a thin, 4 ML pentacene film. d–f) Electric force microscopy (EFM) surface potential images of charge trapping in transistor channels with 4 ML pentacene after application of: d) –5 V, e) –15 V, and f) –40 V to the gate for two minutes. g–i) Corresponding AFM images, measured before the EFM experiments. The yellow arrow in Figure 3d represents the direction of each line scan and the red arrow shows the direction of the overall scan progress. The stars mark the locations where the trap-clearing data presented in Figure 5 were gathered. Charge does not accumulate in the source and drain electrodes, visible as blue regions in the left and right portions of the EFM images. Charged traps are expected to form in the channel between the electrodes and are visible as regions of positive surface potential. In (e) and (f), the traps are scattered and non-uniform, but in (d) trapping is uniform throughout the channel, as we would expect for traps arising from the blanket-deposited precursor (the decrease in voltage from top to bottom is due to slow trap-clearing during the scan).

different morphologies are apparent for the different trap precursors. The most obvious difference is that a greater thickness of DHP (13 ML) was deposited in comparison with the other precursors (1 ML each). This thicker layer was required to confirm the chemical identity of DHP in the transistor channel since 1 ML DHP was not detectable by mass spectrometry, micro-Raman spectroscopy, or transmission IR spectroscopy. The EFM results for 1 ML DHP were identical to those obtained with 13 ML DHP. When deposited thickly, DHP formed needle-like, apparently crystalline features (Figure 3f). The single monolayers of PHO and PQ did not form visible crystalline structures on the sample surface. The uniformity of the PHO deposition is confirmed by the trapping throughout the transistor channel seen in Figure 3d. For all samples, the thin 4 ML films of pentacene show incomplete coverage of the transistor channel and poor wetting of the gold electrodes, yielding tall spire features as in Figure 3g (spires to left and right of the channel).

In the EFM images, Figure 3d–f, charge trapping is observed as regions of positive potential. The 4 ML P + 1 ML PHO sample shows strikingly uniform charge trapping throughout the transistor channel (Figure 3d). The change in potential from top to bottom of the scan is due to traps clearing over the course of the scan, not an overall "hot spot" in the transistor channel: each line scan in the image proceeds from left to right (yellow arrow) and the overall progress of the scan is from top to bottom (red arrow). The lateral nonuniformities in trapping magnitude within the channel can be attributed to variations in coverage (Figure 3g). Note that this level of trapping required only a –5 V gate bias. The 4 ML P + 13 ML DHP sample has traps scattered throughout the transistor channel (Figure 3e), very different from the uniform trapping seen with the PHO precursor. This degree of trapping, which arose from a –15 V gate bias, is similar to that seen in 4 ML P alone with a –15 V gate bias and also similar to that seen in 4 ML P + 1 ML DHP (see Supporting Information). The 4 ML P + 1 ML PQ shows very little trapping (Figure 3f) even with a –40 V gate bias; these traps are clearly related to major topographic defects (Figure 3i). The stars in Figure 3d–f represent the locations where trap-clearing spectra were acquired.

A sample array of the raw trap-clearing data for the P + PHO sample is shown in the supplemental information. Choosing the appropriate fitting procedure for this data was critical because these decays contain information about the trap-clearing mechanism(s) at play. Fitting the surface potential decay transients to only a single exponential yielded poor results, showing no trend vs. wavelength and large error bars. This is not surprising given that the trap decay is too slow for

the sample to reach a common "fully cleared" potential at every wavelength. We can understand this behavior mathematically by considering the expression needed to fit a single exponential decay, Equation (1), where ϕ_i is the initial surface potential and ϕ_f is the final, "fully cleared" surface potential. Expanding Equation (1) yields Equation (2), which would describe the slope of a line approximating a very slow exponential decay.

$$\phi(t) = \phi_f + (\phi_i - \phi_f)\, e^{-kt} = \phi_i e^{-kt} + (1 - e^{-kt})\, \phi_f \quad (1)$$

$$\phi(t) \simeq \phi_i + (\phi_f - \phi_i)\, kt = \phi_i + (\Delta\phi\ k)\, t \quad (2)$$

The fundamental ambiguity in Equation (2) lies in the fact that differences in either ϕ_f or k can alter the slope. If only short-time data is recorded, ϕ_f and k cannot be determined independently. Since the trap-clearing behavior that we measure here is so slow (hundreds of seconds per transient), measuring times long enough for independent determination of ϕ_f and k at 36 wavelengths cannot be practically achieved.

To address this issue, we consider these decays as a sum of two exponentials:

$$\phi(t) = \phi_i - rt + \Delta\phi\ e^{-k_{\exp} t} \quad (3)$$

where we have assumed one of the exponential decays to be very slow compared to the measurement time. In writing Equation (3), we have replaced the $\Delta\phi k$ term in Equation (2) with the slope r. As we later discuss, this separation of the potential decay into a fast and a slow term implies that at least two different mechanisms are responsible for charged trap-clearing in our samples; we will show that the fast exponential decay is mostly light-independent, while the slow (approximately linear) decay is very light-sensitive. To separate these decays in practice, we fit the later two-thirds of the data to the first two terms in Equation (3). Subtracting this best-fit line, the data decayed to zero and was fit to the third term in Equation (3), with $\Delta\phi$ the change in potential due to the fast exponential component and $k_{\exp}$ the exponential decay rate. This line-subtraction procedure effectively separates the trap-clearing behavior at short times (fast, light-insensitive, exponential decay) from the behavior at long times (slow, light-sensitive, linear decay).

The fitting procedure is summarized in **Figure 4** for the 4 ML P + 1 ML PHO sample. Different surface potential decay speeds (trap-clearing rates) are clearly evident for different wavelengths of illumination. The wavelength dependence of the linear slopes and exponential rates is readily extracted and plotted. Note that in Figure 4a,b, we have normalized the slopes and rates by dividing by the energy of the illuminating wavelength in eV. This correction converts the units of the experiment, which was performed at constant incident power, into units that reflect the photon-dependence of the trap-clearing process. We also plot $\Delta\phi$ vs. wavelength. The wavelength dependence of this value would be of interest if it represented the amount of surface potential drop due to the exponential decay. However, the traps are not completely cleared during the experimental period of single-wavelength illumination, so this drop appears relatively larger and larger as the experiment progresses and the traps are filled closer to saturation. It is therefore likely that the observed $\Delta\phi$ value represents some combination of potential drop and trap-saturation history.

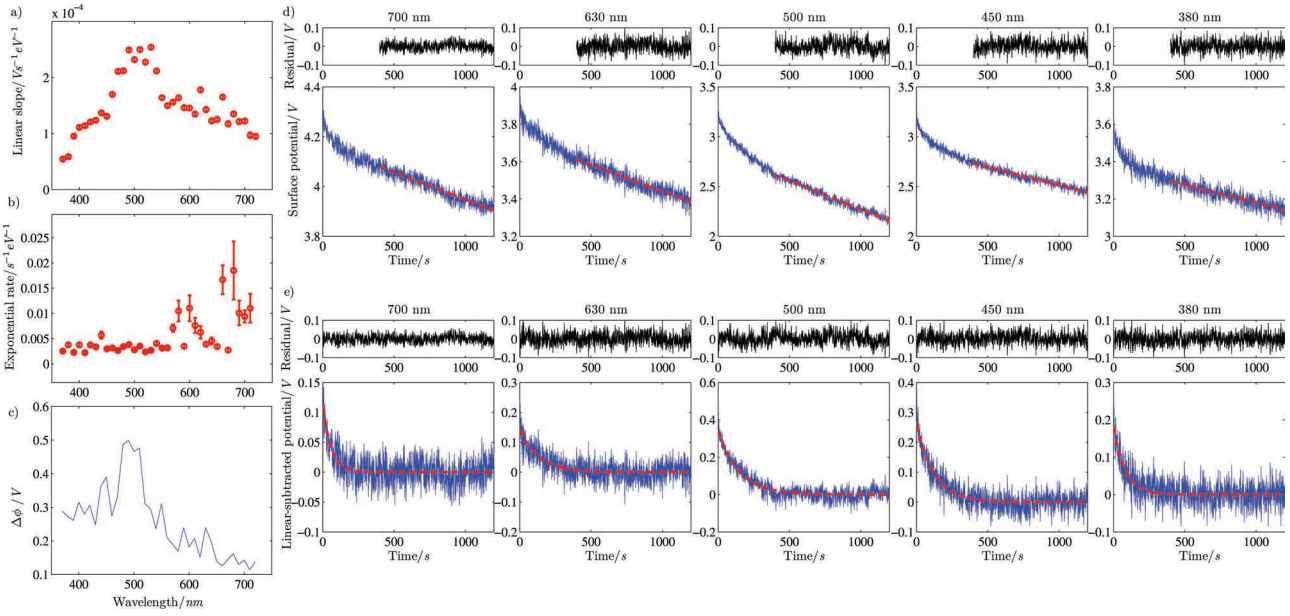

Figure 4. We demonstrate our fitting procedure using this sample set of transients at various wavelengths for charged trap-clearing in the PHO-layered device. The last two-thirds of each decay transient are fitted to a line and the best-fit line is subtracted from the entire transient. The resulting decay curve is fitted to a single exponential function. The rates of these two processes (slow linear and fast exponential) are normalized to the energy of the illumination and plotted vs. wavelength: a) slow linear decay, displayed in units of V s^{-1} eV^{-1}, and b) fast exponential decay, in units of s^{-1} eV^{-1}. The difference between the initial potential and the y-intercept of the best-fit line is plotted in (c) as $\Delta\phi$ vs. wavelength. The apparent variation in $\Delta\phi$ vs. wavelength is likely to be an artificial measure of the device history. Sample fits and residuals for various wavelengths are shown for the linear fits in (d) and for the exponential fit to the linear subtracted data in (e).

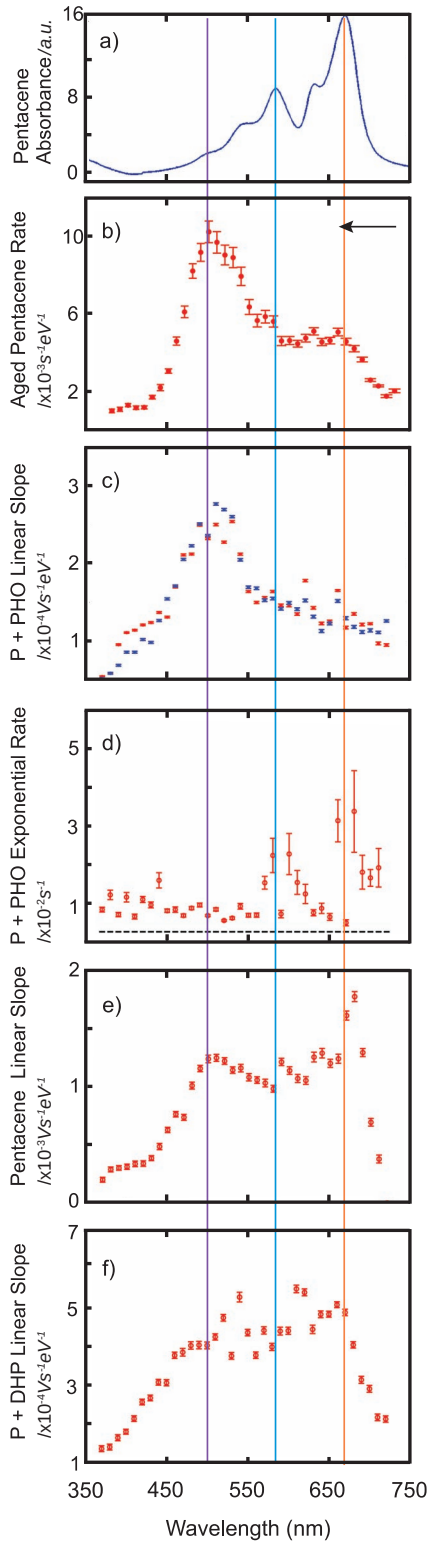

Figure 5. a) Absorption spectrum of pentacene (a.u.). Reproduced with permission.[10] b) Trap-clearing spectrum (exponential rates) in aged pentacene obtained by Luria et al. Reproduced with permission.[10] c) Slope of the slow linear decay vs. wavelength for traps in 4 ML pentacene +1 ML PHO. The blue and red spectra were taken at different locations on the same sample. d) Fast exponential rates vs. wavelength for traps in 4 ML pentacene +1 ML PHO. With no illumination, the trap-clearing in 4 ML pentacene +1 ML PHO is a single exponential decay; the associated decay rate in units of s^{-1} is plotted in black. Note that this trap-clearing spectrum is not normalized to illumination energy as in Figure 4b, for direct comparison with the dark rate. e) Slope of the slow linear decay vs. wavelength for traps in 4 ML pentacene alone. f) Slope of the slow linear decay vs. wavelength for traps in 4 ML pentacene +13 ML DHP. The vertical colored lines are a guide to the eye for comparison with the absorption spectrum of pentacene. The arrow in (b) represents the direction of wavelength scanning for spectra (b–f).

The results of all the trap-clearing experiments are summarized in **Figure 5**. All slopes (Figure 5c,e,f) are normalized to the energy of the illuminating wavelength in eV, as in Figure 4; note that the rate plotted in Figure 5d is not normalized, for direct comparison with the dark trap-clearing rate. The slow linear slopes for trap-clearing in the 4 ML P + 1 ML PHO are plotted as a function of wavelength in Figure 5c. The red and blue spectra represent detrapping experiments performed at two of the several different locations studied in the sample; they agree well. The slow portion of the P + PHO trap-clearing shows a large peak at 500 nm and two smaller features at 660 and 620 nm. In contrast, the fast exponential rates for the P + PHO sample trap-clearing plotted vs. wavelength in Figure 5d do not show a rate enhancement at 500 nm. Instead, the exponential rates are enhanced only at wavelengths where pentacene absorbs. After the light-dependent experiment, a dark decay transient was collected; this decay was exponential and had no linear component. The dark rate for the P + PHO sample is plotted as the dashed line in Figure 5d. However, the P + PHO sample was the only one to show a clear wavelength dependence in the exponential portion of the decay. The fast rates are significantly above the dark rate at 630 nm, but the rate enhancements near 675 nm may not be significant when data taken at multiple locations is compared.

The slow linear slopes for trap-clearing in the 4 ML pristine pentacene are plotted in Figure 5e. This spectrum shows some finer features in the pentacene absorption region, but more importantly, it does not show a relatively large peak at 500 nm. Likewise, the slow linear slopes for 4 ML P + 13 ML DHP are plotted in Figure 5f; this spectrum strongly resembles the analogous pristine pentacene spectrum, and does not show a major peak at 500 nm. The sloping shoulder present at 500 nm in Figure 5e,f is consistent with minor sample aging during sample loading, as discussed below. The traps in the P + PQ sample did not show wavelength dependence in either the fast or slow parts of the surface potential decay, consistent with a non-chemical trapping mechanism.

Before interpreting these results, it is also important to note that several chemical characterization techniques were performed to confirm that the trap-precursors are indeed intact on the transistor substrate. First, to be sure that PHO and DHP did not break down when exposed to the high temperatures required for deposition, we compared the ^{1}H NMR spectra of material recovered from the crucible post-deposition with the corresponding spectra of the fresh material (see supplement). Some PQ is present in the PHO both before and after deposition; this is not surprising since it is the starting material for the PHO synthesis. For both PHO and DHP, we found that no new chemical species appeared as a result of heating. We then

considered the distribution and chemical identity of the trap-precursors on the sample surface. In the case of the PHO-layered sample, the unprecedented uniform trapping everywhere in the transistor channel is clear evidence for the presence of a trap-precursor in the channel. After AFM and EFM analysis, we performed laser desorption ionization (LDI) mass spectrometry on the active region of the sample (see supplement). Consistent with the ^{1}H NMR data, the only chemical species present were those expected: pentacene, PHO, and PQ (starting material for PHO synthesis). A limitation of this work is that no further spectroscopy was performed on the P + PHO sample. This work therefore does not explicitly differentiate between the presence of PHO or its tautomer (pentacene with a central –OH group) on the sample surface. However, since both oxygenated defects are expected to form PHO^+, our conclusions regarding the charged defect species are not affected.[25] In the case of the DHP-layered sample, the topography clearly shows that the precursor layer extends throughout the transistor channel. The chemical identity of this precursor is crucial in the interpretation of the P + PHO trapping results (Figure 2c,d, discussed below). Transmission mode infrared spectroscopy of the transistors probed only the active region of the device due to the small region of illumination allowed by the sample holder and the high reflectivity of the gold electrodes. Codeposition of P and DHP is confirmed by the good agreement between the transition intensities and energies in infrared spectra of the active-region of the transistor structure and similarly prepared neat films, as shown by **Figure 6**. We believe the DHP is deposited with no or minimal degradation; traces of "tetrahydropentacene" (alternating aromatic and aliphatic rings) and 5,14-dihydropentacene may also be present (see Supporting Information), but as our EFM data shows, none of these species appears to be an active trap precursor since uniform trapping is not observed in the DHP sample. For a comparison of experimental and calculated infrared absorption spectra with tentative peak assignments, see the Supporting Information. Additional characterization techniques were not performed on the P + PQ sample since its codeposition with pentacene is well established, and it is not expected to break down under deposition conditions.[30]

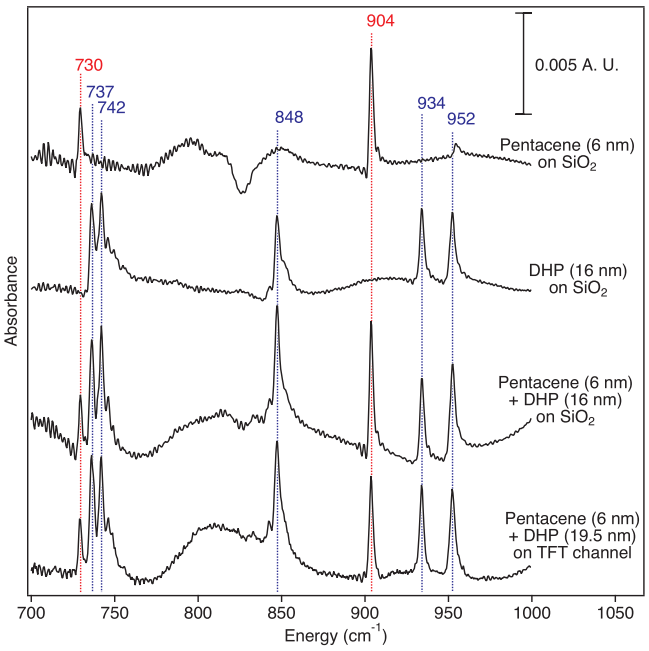

Figure 6. Infrared absorption spectra for, from top to bottom: 4 ML pentacene on SiO_2; 10.7 ML DHP on SiO_2; 4 ML pentacene +10.7 ML DHP on SiO_2; 4 ML pentacene +13 ML DHP on bottom-contact transistor substrate. The first three spectra represent control samples used to confirm the pentacene +DHP sequential deposition procedure; the last spectrum represents the 4 ML pentacene +13 ML DHP transistor before AFM/EFM study. The vertical dotted lines mark the characteristic transitions for pentacene (red; 730 and 904 cm^{-1}) and DHP (blue; 737, 742, 848, 934, and 952 cm^{-1}).

3. Discussion

We first consider the interpretation of the electric force microscopy 2D images in Figure 3. If a defect species/trap-precursor blanket-deposited onto one of our pentacene transistors reacts to form charged traps, then uniform charge trapping throughout the transistor channel is expected in our EFM measurements. This trapping pattern was only present in the P + PHO sample (Figure 3d). The application of only a –5 V gate bias led to 3 V of charge trapping, meaning that 60% of the holes induced in the channel became trapped — an enormous effect. This finding establishes PHO as a potent charged trap-precursor. Although mass spectrometry showed that both PHO and PQ were present on this transistor, PQ has been used as the dielectric in a pentacene transistor,[43] is energetically not likely to form charged traps in pentacene,[30] and the P + PQ transistor exhibits only morphology-defect-related trapping. Therefore, the trapping effect most likely arises from the addition of PHO. However, the proposed reaction of PHO with pentacene charge carriers to form charged defects leads to two different charged species: PHO^+ and DHP^+ (Figure 2c).[10] In order to differentiate between the effects of these two charged species, the charge trapping in the P + DHP transistor must be considered. We used 13 ML DHP for this experiment because 1 ML DHP on 4 ML pentacene was not detectable with mass spectrometry, micro-Raman spectroscopy, or transmission IR spectroscopy, and it was crucial that we confirm the chemical identity of the precursor spectroscopically since DHP is predicted to yield only DHP^+ upon reaction with pentacene charge carriers. The P + DHP transistor did not show readiness or uniformity of trapping, suggesting that the traps formed in this sample arise from a mechanism besides formation of DHP^+. Tello et al. observed irreversible trapping in regions of pentacene film discontinuity;[44] the traps in the P + DHP sample may arise from a similar effect since 4 ML pentacene on our transistor substrates does not form a completely continuous film (see Supporting Information), although we cannot be certain of this since the thick layer of DHP obscures the pentacene morphology in our AFM measurement. Nevertheless, the trapping observed in the P + DHP transistor is not consistent with traps arising from a blanket-deposited trap-precursor. This strongly suggests that PHO^+ is responsible for the trapping induced by addition of PHO to pentacene, and that DHP^+ is not.

The results of the trap-clearing spectra, Figure 5, support the assignment of PHO^+ as the chemical trap species and yield further evidence for multiple trap-clearing mechanisms in pentacene.[10] First, we consider the wavelength dependence of the slow, linear portions of the decay transients (Figure 5c,e,f). Consistent with our interpretation of the EFM data, only the P + PHO sample (Figure 5c) exhibited strongly enhanced trap-clearing rates at 500 nm. We attribute this rate enhancement to the excitation of the charged trap species, followed by neutralizing charge transfer from pentacene.[10] This behavior was reproducible in multiple locations in the transistor channel, consistent with the trapping uniformity implied by the EFM data. Furthermore, the peak at 500 nm in the P + PHO trap-clearing spectrum reproduces both the peak observed by Luria et al. in aged pentacene (Figure 5b) and the TD-DFT calculated absorption spectrum of PHO^+ (Figure 2b).[10] PHO^+ is therefore likely both the cause of the charge trapping we observe and the electronically active degradation defect in aged pentacene.

In contrast, the P + DHP (Figure 5f) trap-clearing spectrum strongly resembled that of freshly deposited pristine pentacene (Figure 5e) and did not match the either of the predicted charged trap absorption spectra (Figure 2b). Instead of a dramatic rate enhancement at 500 nm, both of these spectra (Figure 5e,f) have a "shoulder" at or near 500 nm, which we attribute to the presence of a trace amount of PHO^+ in the samples. A small amount of pentacene oxidation in such thin films is not surprising since the samples were all briefly exposed to ambient conditions while they were loaded into our custom AFM/EFM microscope. These spectra support our assertion that DHP^+ is not a chemical charged trap in pentacene. The P + PQ sample did not show any wavelength dependent trap-clearing behavior, consistent with non-chemical trapping in the P + PQ sample.

Besides the feature at 500 nm, the slow-portion trap-clearing spectra (Figure 5c,e,f) exhibit some fine structure at longer wavelengths. We tentatively assign these features to enhancements in trap-clearing rate due to excitation of pentacene leading to excited-electron transfer that neutralizes the charged trap species. The trap-clearing spectra thus provide evidence for the operation of both proposed light-induced trap-clearing mechanisms (excitation of pentacene or of the charged trap species, followed by neutralizing charge transfer to the trap). The larger magnitude of the peak at 500 nm implies that excitation of PHO^+ is more effective than excitation of pentacene in initiating trap-clearing. Although this rate enhancement is qualitatively reasonable since the charge transfer to excited PHO^+ is expected to be more exothermic (see supplement), we caution that the rate of electron transfer also depends on reorganization energy and an orbital overlap integral, the calculation of which are beyond the scope of our paper. We further note that this charge transfer is only the first step in fully stabilizing the charged defect (to return to PHO, the reactions in Figure 2c must be reversed).

A fast, exponential decay component is observed in all the samples, but only in the P + PHO sample was this component wavelength-dependent. The P + PHO sample had enhanced exponential decay rates at wavelengths where pentacene absorbs. This is puzzling because if the exponential component of the trap-clearing is due to pentacene absorption, we would expect to see the same pentacene-related wavelength dependence of the exponential rates in *all* the samples, not just one. In contrast, the exponential decay component does not depend on illuminating wavelength in the pentacene-only, P + DHP, and P + PQ samples. This fast (a few tens of seconds), wavelength-independent decay cannot be attributed to trap clearing via thermal excitation of pentacene, which is expected to be very slow (many hours).[11] Trap-clearing in intergrain traps has been shown to be light-insensitive, but the time scale for intergrain trap-clearing is much slower (greater than 24 hours) than the fast exponential clearing we observe.[44] Recently, evidence has been reported for proton migration into SiO_2[45,46] and for hole states in amorphous dielectrics;[47] trap-clearing of charges near the surface in the dielectric might explain the light-independent fast clearing we observe in these samples. However, none of these cases explains why only P + PHO would exhibit a pentacene-absorption-dependent exponential decay. One possibility could be that there really is an additional and distinct fast trap-clearing mechanism in this sample. Perhaps PHO accepts electrons from optically excited pentacene more readily in some configurations or local environments than others; a scenario like this could yield two light-sensitive trap-clearing processes. At this point, it is unclear whether or not a third trap-clearing mechanism (beyond optical absorption by pentacene or the charged trap species) is needed to fully explain the fast single-exponential decay portion of the data.

4. Conclusions

In summary, we have layered thin pentacene films with pentacene trap-precursor candidates, imaged the trapped charge concentration in these samples, and detected light-dependent trap-clearing rates at selected sample locations with time- and wavelength-resolved electric force microscopy. We have demonstrated that PHO is capable of readily producing large charge trapping effects in pentacene that directly and strikingly verify the predicted charge clearing spectrum.[10] These observations, coupled with the control experiments in DHP, strongly indicate that PHO^+ (and not DHP^+) is responsible for chemical, light-responsive charge trapping in pentacene thin film devices. The agreement between the trap-clearing spectra of the P + PHO sample and aged pentacene also strongly suggests that the trapping effects are the same, i.e., PHO^+ is likely the charged defect that forms in aged pentacene devices. This result contradicts the general understanding of charged traps in pentacene as arising from DHP or PQ, and is also surprising because DHP^+ is expected to be a thermodynamically more stable trap species than PHO^+.[25] More generally, this result should be of interest in the design of new organic semiconductors. Strategies for developing new *n*-channel materials are strongly based in meeting specific electron affinities predicted to limit reaction with oxygen.[48,49] For example, the growing family of naphthalene and perylene diimides are not expected to undergo degradation under atmospheric conditions, especially with electron-withdrawing core substituents to lower the LUMO level and stabilize the radical anion. However, positive threshold voltage shifts indicating charge trapping

are still observed in these materials, and neither the chemical nature of this trapping nor the role of impurities due to degradation during deposition has yet been spectroscopically investigated.[50,51] Our work demonstrates that in predicting and understanding air sensitivity, reactivity, and degradation-related charge trapping processes, thermodynamic considerations alone may not be sufficient. Our work also shows that EFM is a useful tool in studying these issues.

5. Experimental Section

Sample Preparation: Pentacene for deposition was obtained from Kintec, HK (triple sublimed grade). 6,13-pentacenequinone (PQ) for deposition and for synthesis of pentacen-6(13H)-one (PHO) was obtained from Aldrich. Pentacene used for synthesis of 6,13-dihydropentacene (DHP) was obtained from VWR International. All commercially obtained chemicals were used without further purification.

Synthesis of pentacen-6(13H)-one (PHO) was based on procedures from the literature: PQ was heated to reflux in dry THF with sodium borohydride to yield 6,13-dihydroxypentacene (13% after column chromatography);[52] 6,13-dihydroxypentacene was then heated to reflux in 100:1 THF:HCl to give PHO (18%).[53] ^{1}H NMR ($CDCl_3$, 500 MHz): δ8.97 ppm (s, 2H); 8.07 ppm (d, 2H); 7.96 (d, 2H); 7.89 ppm (d, 2H); 7.61 ppm (t, 2H); 7.53 ppm (t, 2H); 4.71 ppm (s, 2H). Monitoring a sample of the purified PHO by thin film chromatography over the course of a day revealed the appearance of an unidentified second species. The PHO used in these experiments was therefore prepared fresh on the day of sample preparation. The freshly purified compound was stored under argon and cold for less than 2 hours before being transferred to the glove box housing the evaporator for sample preparation.

Synthesis of 6,13-dihydropentacene (DHP) was based on procedures[54] and characterization data[55] from the literature. Pentacene was mixed with HI and glacial acetic acid and heated to reflux for 24 hours in dark under N_2. The reaction was quenched with sodium bisulfite and DHP was separated from the reaction mixture by column chromatography (17%). ^{1}H NMR ($CDCl_3$, 600 MHz): δ7.82 ppm (t, 8H); 7.44 ppm (dd, 4 H); 4.27 ppm (s, 4H).

Bottom-contact transistor substrates were fabricated by thermally growing 315 nm SiO_2 on an n-type Si wafer (1–10 Ωcm) and patterning interdigitated gold source and drain electrodes (5 µm channel length, 150 cm channel length, 15 µm electrode width, 3 × 6 mm total active area) using standard photolithography techniques. The cleaning protocol for substrates is as follows: Bottom-contact substrates were rinsed with acetone and IPA, sonicated in acetone, and soaked in microposit remover fluid 1165 (Shipley) for at least 8 hours to remove the protective coating of photoresist; they were then rinsed with acetone and IPA before undergoing 10 minutes UV-ozone cleaning and additional sonication in acetone and IPA. All substrates were then sonicated in nonionic detergent (Aquet), dried, and UV-ozone cleaned 10 minutes more.

Substrates were heated to 60 °C during PHO deposition and all pentacene depositions except for the pentacene + PQ trial and the IR control sample. Substrates were not heated for PQ or DHP deposition. Source material was resistively heated in a ceramic crucible to achieve deposition rates of approximately 0.1 Å/s. 60 Å (nominally 4 monolayers, 4 ML, measured by quartz crystal microbalance) pentacene was deposited first. For trap-precursor candidates PQ and PHO, ~1 ML (nominally 15 Å) trap candidate was deposited next; for DHP, ~13 ML (nominally 195 Å) was deposited on the pentacene film. Vacuum was broken and samples were exposed to the glove box N_2 atmosphere between deposition of pentacene and the trap-precursor in order to remove the pentacene-only samples and place clean substrates for trap-precursor-only controls.

Electric Force Microscopy (EFM): Atomic force microscopy (AFM), EFM, and wavelength-dependent trap-clearing measurements were performed under high vacuum (1–2 × 10^{-6} mbar) with transistor source, drain, and gate grounded. Samples were briefly exposed to ambient light and atmosphere (less than 30 minutes) while they were loaded into the microscope. A Ti-Pt coated Si cantilever was used (MikroMasch, NSC18 series, resonant frequency f = 75 kHz, spring constant k = 3.5 N m^{-1}). Cantilever deflection was measured using a fiberoptic interferometer with operating wavelength 1310 nm. Frequency demodulation was achieved using a PLLPro AFM controller (RHK), providing a voltage output proportional to the cantilever frequency shift δf.

Bottom-contact transistor substrates with sequentially deposited pentacene and a trap-precursor were characterized by tapping-mode AFM and EFM. Immediately prior to EFM measurements, traps were populated by applying a negative gate bias for two minutes. Upon returning gate to ground, remaining trapped holes appeared as regions of positive surface potential. Neither a gate bias nor a source-drain bias was applied during all AFM and EFM imaging. Modulated EFM was used to image surface potential (Figure 1b), and swept-voltage EFM was used to measure surface potential during trap-clearing experiments (Figure 1c).[9]

In modulated EFM (used in Figure 1b), both an AC modulation voltage (ω, 2-3 V rms) and a DC potential were applied to the cantilever. The first (ω) and second (2ω) Fourier components of the cantilever frequency shift due to the modulation frequency were monitored by lock-in detection (Stanford Research Systems, 30 ms time constant, and Perkin Elmer, 50 ms, respectively) with a sensitivity of 1 V. The first component of the cantilever frequency with applied AC and DC potential is related to the DC potential and the tip-sample contact potential through the relationship:

$$\hat{f}(\omega) = \frac{f_0 V_{T,AC}}{2k_0}\frac{\partial^2 C}{\partial z^2}(V_{T,DC} - \phi) \quad (4)$$

where f_0 is the cantilever resonance frequency, k_0 is the cantilever spring constant, $V_{T,AC}$ and $V_{T,DC}$ are the AC and DC components of the tip potential, $\partial^2C/\partial z^2$ is the second derivative of tip-sample capacitance with respect to cantilever position, and ϕ is the tip-sample contact potential difference. The output of a PID (Stanford Research Systems SIM960 Analog PID Controller, P = –0.1, I = 80 Hz, D = 5 ×10^{-4} s) feeding back on the DC potential ($V_{T,DC}$) to nullify the first component of the frequency shift in Equation (4) is equal to the tip-sample contact potential as mapped in Figure 3. The cantilever was scanned in the plane 60 nm above the sample plane (topography is not followed).

In swept voltage EFM (used in Figure 1c), a series of DC potentials (usually –3 to 3 V) was applied to the cantilever and the cantilever frequency shift was measured at each point. This produced a parabolic frequency shift-tip voltage curve with a maximum where the applied voltage is equal to the tip-sample contact potential, through the relationship:

$$\delta f(V_T) = f_0 - \frac{f_0}{4k_0}\frac{\partial^2 C}{\partial z^2}(V_T - \phi)^2 \quad (5)$$

with f_0 the cantilever resonance frequency, k_0 the cantilever spring constant, V_T the cantilever tip potential, $\partial^2C/\partial z^2$ the second derivative of tip-sample capacitance with respect to cantilever position, and ϕ the tip-sample contact potential difference. The surface potential was measured by extracting the maxima of these frequency shift – tip voltage parabolas (Equation 5). This process is quite slow compared to modulated EFM. Modulated EFM was used for 2D imaging. Swept-voltage EFM was used for measuring the surface potential over a single location over time (trap-clearing experiments).

In the trap-clearing experiments, the swept-voltage EFM measurement of the surface potential was repeated at 2 Hz for up to 1200 seconds, producing a surface potential decay transient. After measurement of the transient, traps were freshly repopulated by biasing the gate at –5, –10, –20, or –40 V (PHO, DHP, pentacene, and PQ samples, respectively) for 120 seconds before beginning the next transient measurement. The charged traps in the PHO and DHP samples were so slow to clear that traps were further cleared by a white-light LED (10 seconds and 8 seconds, respectively) between transient measurements and before trap

repopulation. This procedure did not yield a consistent initial surface potential for each measurement. If the traps are not sufficiently cleared by the single-wavelength light (or by additional LED illumination), a different initial surface potential will be produced by the next gate bias. A decay transient was measured for each of 36 wavelengths between 370 and 750 nm. The cantilever was maintained in position 60–120 nm (dependent on the sample topography) above the charged trap site under study during transient measurement. A "dark" spectrum was obtained for each sample by measuring the surface potential as a function of time without illumination. The magnitude of this dark decay rate is strongly dependent on when the scan is performed relative to the light-dependent trap-clearing experiment: if performed first, traps may not be fully saturated for the given gate voltage, resulting in an artificially fast clearing rate. The dark clearing data shown in Figure 5c was collected after the light-dependent experiment. The light source for variable-wavelength illumination was a Dolan-Jenner Fiber-Lite with a 150 W bulb (Ushio) connected to a scanning monochromator (Monoscan 2000, Micropack) and attenuator (Oz Optics). The sample was illuminated with visible light from a 50 µm fiber with numerical aperture 0.22 angled 30° away from horizontal towards the cantilever and roughly 200 µm away from the cantilever tip. The illumination had a measured bandwidth of 5 nm and a measured power of 0.015 µW cm^{-2}. We estimate the intensity of the illumination to be 0.05 mW cm^{-2} at the sample.

Miscellaneous Characterization: Transistor characterization was performed under high vacuum in the same apparatus as AFM and EFM measurements with the cantilever far removed from the sample surface. Current-voltage characteristics were measured by varying the drain current from 10 V to –30 V and keeping source grounded. These measurements were repeated for 16 gate biases between 10 V and –50 V; this data is shown in the supplementary information. We expect low performance in our devices due to the bottom-contact geometry, untreated SiO_2, and low material coverage. For the pentacene transistor used in this study, we observed a clear gating effect, but the device had nonlinear turn-on behavior (usually indicating poor contacts) and did not reach saturation. The low coverage required for our charge-trapping experiments is likely responsible for these non-idealities, especially the contact effects. Although neither the saturation nor the linear-mobility regime was achieved, we calculated the mobilities μ_{sat} and μ_{linear} and from these we estimate a hole mobility on the order of 10^{-4} $cm^2V^{-1}s^{-1}$ in our 4 ML pentacene device.

Mass spectrometry was performed using a MALDI Micro MX time-of-flight benchtop mass spectrometer (Waters) with a 10 Hz N_2 UV laser in positive ion reflectron detection mode. 50-70 individual spectra from each sample were combined for data analysis.

^{1}H NMR spectra were measured for PHO and DHP at 499.76 MHz and 599.50 MHz, respectively. 16 scans of 2 seconds each with a 1 second relaxation decay were acquired for each sample, and the final spectra were zero-filled to 32k or 64k data points. An exponential window function (line broadening) of 0.3 to 1.0 Hz was applied prior to Fourier Transform. Chemical shift values are referenced relative to 7.26 ppm ($CDCl_3$).

To identify infrared transitions characteristic of P and DHP, 4 ML (6 nm) of pentacene, 10.7 ML (16 nm) of DHP, or sequential layers of the two materials (4 ML pentacene + 10.7 ML DHP) were deposited on a 520 nm thick thermal oxide grown on 500 µm thick, single-side-polished, n-type Si substrates. Infrared spectra of an approximately 2.5 mm × 6 mm region of each sample were obtained at normal incidence and 1 cm^{-1} resolution in transmission mode with a nitrogen-purged FTIR spectrometer equipped with a mercury-cadmium-telluride detector. The reported spectra consist of 2000 coadded scans referenced to spectra of a similarly prepared, film-free oxidized sample. Interference fringes in the spectra were removed computationally.[56]

Infrared spectra of transistor structures were taken in a similar fashion, with the infrared radiation only probing the active region of the device. This was ensured both by the design of the sample holder as well as the reflective nature of the 35 nm thick gold electrodes. The reported spectra were referenced to a similarly prepared, film-free transistor structure.

Supporting Information

Supporting Information is available from the Wiley Online Library or from the author.

Acknowledgements

The authors would like to thank Anthony Condo for the acquisition of the ^{1}H NMR spectra and assistance with the mass spectrometry. This work made use of the soft matter characterization facility of the Cornell Center for Materials Research (CCMR) with support from the National Science Foundation Materials Research Science and Engineering Centers (MRSEC) program (DMR 1120296). A portion of this work was performed at the Cornell NanoScale Facility, a member of the National Nanotechnology Infrastructure Network, which is supported by the National Science Foundation (Grant ECS-0335765). L.M.S. acknowledges support from an NSF Graduate Research Fellowship and NSF-DMR 1006633. V.A.P. acknowledges the support of the CCMR, NSF-DMR 1120296. J.L.L. and J.A.M. acknowledge the support of NSF-DMR 1006633.

Received: March 1, 2012
Revised: July 7, 2012
Published online: August 8, 2012

[1] G. G. Malliaras, V. Krasnikov, H. J. Bolink, G. Hadziioannou, *Appl. Phys. Lett.* **1995**, *66*, 1038–1040.
[2] W. You, Z. Hou, L. Yu, *Adv. Mater.* **2004**, *16*, 356–360.
[3] S. Wang, C.-W. Leung, P. K. L. Chan, *Org. Electron.* **2010**, *11*, 990–995.
[4] V. Bliznyuk, S. Carter, J. Scott, G. Klarner, R. Miller, D. Miller, *Macromolecules* **1999**, *32*, 361–369.
[5] L. J. Soltzberg, J. D. Slinker, S. Flores-Torres, D. A. Bernards, G. G. Malliaras, H. D. Abruna, J.-S. Kim, R. H. Friend, M. D. Kaplan, V. Goldberg, *J. Am. Chem. Soc.* **2006**, *128*, 7761–7764.
[6] O. G. Reid, G. E. Rayermann, D. C. Coffey, D. S. Ginger, *J. Phys. Chem. C* **2010**, *114*, 20672–20677.
[7] T. N. Ng, J. A. Marohn, M. L. Chabinyc, *J. Appl. Phys.* **2006**, *100*, 084505.
[8] M. Jaquith, E. M. Muller, J. A. Marohn, *J. Phys. Chem. B* **2007**, *111*, 7711–7714.
[9] M. J. Jaquith, J. E. Anthony, J. A. Marohn, *J. Mater. Chem.* **2009**, *19*, 6116–6123.
[10] J. L. Luria, K. A. Schwarz, M. J. Jaquith, R. G. Hennig, J. A. Marohn, *Adv. Mater.* **2011**, *23*, 624–628.
[11] D. V. Lang, X. Chi, T. Siegrist, A. M. Sergent, A. P. Ramirez, *Phys. Rev. Lett.* **2004**, *93*, 076601.
[12] C. Goldmann, D. J. Gundlach, B. Batlogg, *Appl. Phys. Lett.* **2006**, *88*, 063501.
[13] W. L. Kalb, K. Mattenberger, B. Batlogg, *Phys. Rev. B: Condens. Matter* **2008**, *78*, 035334.
[14] O. Jurchescu, J. Baas, T. Palstra, *Appl. Phys. Lett.* **2005**, *87*, 052102.
[15] F. D. Angelis, M. Gaspari, A. Procopio, G. Cuda, E. D. Fabrizio, *Chem. Phys. Lett.* **2009**, *468*, 193–196.
[16] B. Stevens, S. Perez, J. Ors, *J. Am. Chem. Soc.* **1974**, *96*, 6846–6850.
[17] A. Maliakal, K. Raghavachari, H. Katz, E. Chandross, T. Siegrist, *Chem. Mater.* **2004**, *16*, 4980–4986.
[18] A. Reddy, M. Bendikov, *Chem. Commun.* **2006**, 1179–1181.
[19] S. Chien, M. Cheng, K. Lau, W. Li, *J. Phys. Chem. A* **2005**, *109*, 7509–7518.
[20] L. Tsetseris, S. T. Pantelides, *Phys. Rev. B: Condens. Matter* **2007**, *75*, 153202.

[21] H. Najafov, D. Mastrogiovanni, E. Garfunkel, L. C. Feldman, V. Podzorov, *Adv. Mater.* **2011**, *23*, 981–985.
[22] L. Tsetseris, S. T. Pantelides, *Phys. Rev. B: Condens. Matter* **2008**, *78*, 115205.
[23] L. Tsetseris, S. Pantelides, *Org. Electron.* **2009**, *10*, 333–340.
[24] M. Yamada, I. Ikemoto, H. Kuroda, *Bull. Chem. Soc. Jpn.* **1988**, *61*, 1057–1062.
[25] J. Northrup, M. Chabinyc, *Phys. Rev. B: Condens. Matter* **2003**, *68*, 041202.
[26] C. C. Mattheus, J. Baas, A. Meetsma, J. L. d. Boer, C. Kloc, T. Siegrist, T. T. M. Palstra, *Acta Crystallogr. E: Structure Rep. Online* **2002**, *58*, o1229–o1231.
[27] L. Roberson, J. Kowalik, L. Tolbert, C. Kloc, R. Zeis, X. Chi, R. Fleming, C. Wilkins, *J. Am. Chem. Soc.* **2005**, *127*, 3069–3075.
[28] B. H. Northrop, J. E. Norton, K. N. Houk, *J. Am. Chem. Soc.* **2007**, *129*, 6536–6546.
[29] O. Jurchescu, J. Baas, T. Palstra, *Appl. Phys. Lett.* **2004**, *84*, 3061–3063.
[30] E. Gomar-Nadal, B. R. Conrad, W. G. Cullen, E. A. Willams, *J. Phys. Chem. C* **2008**, *112*, 5646–5650.
[31] B. R. Conrad, E. Gomar-Nadal, W. G. Cullen, A. Pimpinelli, T. L. Einstein, E. D. Williams, *Phys. Rev. B: Condens. Matter* **2008**, *77*, 205328.
[32] I. Salzmann, R. Opitz, S. Rogaschewski, J. P. Rabe, N. Koch, B. Nickel, *Phys. Rev. B: Condens. Matter* **2007**, *75*, 174108.
[33] I. Salzmann, S. Duhm, R. Opitz, J. P. Rabe, N. Koch, *Appl. Phys. Lett.* **2007**, *91*, 051919.
[34] O. Berg, E. Chronister, T. Yamashita, G. Scott, R. Sweet, J. Calabrese, *J. Phys. Chem. A* **1999**, *103*, 2451–2459.
[35] P.Coppo, S. Yeates, *Adv. Mater.* **2005**, *17*, 3001–3005.
[36] B. Purushothaman, S. R. Parkin, J. E. Anthony, *Org. Lett.* **2010**, *12*, 2060–2063.
[37] M. Kiguchi, M. Nakayama, T. Shimada, K. Saiki, *Phys. Rev. B: Condens. Matter* **2005**, *71*, 035332.
[38] R. Ruiz, A. Papadimitratos, A. Mayer, G. Malliaras, *Adv. Mater.* **2005**, *17*, 1795.
[39] B.-N. Park, S. Seo, P. G. Evans, *J. Phys. D: Appl. Phys.* **2007**, *40*, 3506–3511.
[40] H. Yang, L. Yang, M.-M. Ling, S. Lastella, D. D. Gandhi, G. Ramanath, Z. Bao, C. Y. Ryu, *J. Phys. Chem. C* **2008**, *112*, 16161–16165.
[41] M. Fiebig, D. Beckmeier, B. Nickel, *Appl. Phys. Lett.* **2010**, *96*, 083304.
[42] A. Shehu, S. D. Quiroga, P. D'Angelo, C. Albonetti, F. Borgatti, M. Murgia, A. Scorzoni, P. Stoliar, F. Biscarini, *Phys. Rev. Lett.* **2010**, *104*, 246602.
[43] O. D. Jurchescu, M. Popinciuc, B. J. van Wees, T. T. M. Palstra, *Adv. Mater.* **2007**, *19*, 688.
[44] M. Tello, M. Chiesa, C. M. Duffy, H. Sirringhaus, *Adv. Funct. Mater.* **2008**, *18*, 3907–3913.
[45] A. Sharma, S. G. J. Mathijssen, T. Cramer, M. Kemerink, D. M. de Leeuw, P. A. Bobbert, *Appl. Phys. Lett.* **2010**, *96*, 103306.
[46] A. Sharma, S. G. J. Mathijssen, E.C. P. Smits, M. Kemerink, D. M. de Leeuw, P. A. Bobbert, *Phys. Rev. B: Condens. Matter* **2010**, *82*, 075322.
[47] B. Lee, A. Wan, D. Mastrogiovanni, J. E. Anthony, E. Garfunkel, V. Podzorov, *Phys. Rev. B: Condens. Matter* **2010**, *82*, 085302.
[48] C. Newman, C. Frisbie, D. da Silva, J. Bredas, P. Ewbank, K. Mann, *Chem. Mater.* **2004**, *16*, 4436–4451.
[49] Y.-C. Chang, M.-Y. Kuo, C.-P. Chen, H.-F. Lu, I.Chao, *J. Phys. Chem. C* **2010**, *114*, 11595–11601.
[50] B. Jones, M. Ahrens, M. Yoon, A. Facchetti, T. Marks, M. Wasielewski, *Angew. Chem. Int. Ed.* **2004**, *43*, 6363–6366.
[51] X. Zhan, A.Facchetti, S. Barlow, T. J. Marks, M. A. Ratner, M. R. Wasielewski, S. R. Marder, *Adv. Mater.* **2011**, *23*, 268–284.
[52] N. Vets, M. Smet, W. Dehaen, *Tetrahedron Lett.* **2004**, *45*, 7287–7289.
[53] T. R. Criswell, B. H. Klanderman, *J. Org. Chem.* **1974**, *39*, 770–774.
[54] A. J. Athans, J. B. Briggs, W. Jia, G. P. Miller, *J. Mater. Chem.* **2007**, *17*, 2636–2641.
[55] M. Tamano, J. Koketsu, *Bull. Chem. Soc. Jpn.* **1985**, *58*, 2577–2580.
[56] M. Faggin, M. Hines, *Rev. Sci. Instrum.* **2004**, *75*, 4547–4553.